5-2017

A Stochastic Model for Water-Vegetation Systems and the Effect of Decreasing Precipitation on Semi-Arid Environments

Shannon A. Dixon
Utah State University

A STOCHASTIC MODEL FOR WATER-VEGETATION SYSTEMS AND THE EFFECT OF DECREASING PRECIPITATION ON SEMI-ARID ENVIRONMENTS

by

Shannon A. Dixon

A thesis submitted in partial fulfillment
of the requirements for the degree

of

MASTER OF SCIENCE

in

Mathematics

Approved:

Luis F. Gordillo, Ph.D. Major Professor	Brynja Kohler, Ph.D. Committee Member
Patrick Belmont, Ph.D. Committee Member	Mark R. McLellan, Ph.D. Vice President for Research and Dean of the School of Graduate Studies

UTAH STATE UNIVERSITY
Logan, Utah

2017

ABSTRACT

A Stochastic Model for Water-Vegetation Systems
and the Effect of Decreasing Precipitation
on Semi-Arid Environments

by

Shannon A. Dixon, Master of Science
Utah State University, 2017

Major Professor: Luis F. Gordillo, Ph.D.
Department: Mathematics & Statistics

Current climate change trends are affecting the magnitude and recurrence of extreme weather events. In particular, several semi-arid regions around the planet are confronting more intense and prolonged lack of precipitation, slowly transforming these regions into deserts. In this thesis we present a stochastic (meso-scale) model for vegetation-precipitation interactions for semi-arid landscapes. Extensive simulations with the model suggest that persistence in current trends of precipitation decline in semi-arid landscapes may expedite desertification processes by up to several decades.

(61 pages)

PUBLIC ABSTRACT

A Stochastic Model for Water-Vegetation Systems
and the Effect of Decreasing Precipitation
on Semi-Arid Environments

Shannon A. Dixon

Current climate change trends are affecting the magnitude and recurrence of extreme weather events. In particular, several semi-arid regions around the planet are confronting more intense and prolonged lack of precipitation, slowly transforming these regions into deserts. Many mathematical models have been developed for purposes of analyzing vegetation-water interactions, particularly in semi-arid landscapes. Most models are based on the average behavior of the system as a whole, and how it is influenced by external changes. These models may be termed "macro-scale" models. Other models have concerned themselves with the interactions between individuals, in this case the interactions between individual plants and the available water. These models may be termed "micro-scale" models. In this thesis we present a model for vegetation-precipitation interactions which is intermediate between these two types of models. This "meso-scale" model, also known as a stochastic model, has the advantage of incorporating the behavior of the system as a whole, while still retaining the "noise" (or internal influences) from the individual interactions. Extensive simulations with this model suggest that persistence in current trends of precipitation decline in semi-arid landscapes may expedite desertification processes by up to several decades.

To Jarom & Kareste, my greatest blessings. I am a lucky mom!

ACKNOWLEDGMENTS

First of all I would like to express my gratitude to my advisor, Dr. Luis Gordillo. Without his guidance and help, (and infinite patience!), this thesis would not exist. It has been my great privilege to work with you. I also greatly appreciate my committee members, Dr. Brynja Kohler and Dr. Patrick Belmont, for their time and assistance with this project.

I am also very thankful for the funding I received from Utah State University's Research and Graduate Studies, as well as from Dr. Luis Gordillo.

I would be remiss if I did not thank all the professors who have taught me mathematics at USU. I have learned from each of you; thank you for sharing your time and knowledge with me. In particular, I would like to thank Ted Campbell for his early encouragement; you influenced me more than you know.

I would also like to thank my family: first, my children who patiently put up with a part-time mom for half their lives, and who ate more fast food than children should ever have to; and second, my parents for believing in me and for patiently providing moral support and encouragement.

Lastly, I would like to thank my Heavenly Father for the gifts and talents and opportunities with which He has blessed me. Every time I thought a door was closed, He opened a window. I am forever grateful.

Shannon A. Dixon

CONTENTS

LIST OF TABLES

LIST OF FIGURES

CHAPTER 1

INTRODUCTION

1.1 Background

Large regions in the Western United States, Africa, and other parts of the world, are classified as arid or semi-arid environments, characterized in part by their limited and variable pulses of precipitation [6]. Availability of water plays a dominant role in arid and semi-arid regions, which are expected to receive an average of 10 to 30 inches of precipitation annually ($\approx 254 - 508$ kg H_2O $m^{-2}year^{-1}$).

Various methods are used for classifying regions as arid, semi-arid, hyper-arid, desert, etc. A defining characteristic of drylands is lack of precipitation. However, lack of rainfall alone is insufficient for defining boundaries between environments. Comparison of different areas which receive the same amount of annual rainfall reveal a wide variety of vegetation, from grasses and shrublands to heavily forested environments. Thus, water balance (the balance between available water and evapotranspiration) is commonly used for determining aridity of a region [19]. We assume a semi-arid environment has a pronounced dry season, with rainfall concentrated during certain times of the year. The model we will derive provides for both water supply and evaporation, though for simplicity it does not distinguish between sources of water.

According to Sheffield and Wood [23], the 1970s marked a switch to drying trends in soil moisture globally, and particularly in the northern latitudes. Though there are many indirect factors of drought, temperature and particularly precipitation are the primary driving factors. Higher temperatures lead to increases in evapotranspiration and decreased soil moisture. Temperatures are expected to increase, while precipitation is expected to fluctuate according to region. However, in many regions, temperature and precipitation are negatively correlated, leading to predictions of greater occurrence of drought. Overall,

climate change is predicted to increase the intensity and frequency of droughts globally [23].

In particular, average precipitation in the Southwestern United states and other regions of similar climate is predicted to change dramatically in response to global warming [6]. As of August 2016, abnormally dry to moderate drought conditions were observed in large portions of the Western United States, with regions that range between severe to extreme drought occurring in the northern areas, and severe to exceptional drought extending from California into Nevada [20].

The decline in precipitation combined with overall higher temperatures puts indigenous species of plants and animals in semi-arid environments under unusual stress and the parallel habitat loss might pose a threat to local biodiversity [15]. Management strategies should focus on these areas.

Under these circumstances, predicting possible responses of vegetation biomass in semi-arid landscapes to long term changes in precipitation is of profound importance in creating management strategies. Understanding how precipitation affects vegetation in arid and semi-arid environments can aid in designing adaptation and conservation policies to solve environmental problems caused by climate change and land use. [6, 10].

Predicting these responses ultimately depends on interpreting how individuals and populations respond to precipitation [6]. Estimation of the expected time of transition from a vegetative state to bare-soil, as a conceivable measure of those responses, presents several difficulties due to the enormous complexities associated with water-vegetation systems. However, results from simulations of simplified mathematical models could offer a hint on the relationship with the parameters that might drive the decline.

Extensive mathematical modeling and analysis of semi-arid water-vegetation systems has emerged in the last few years, especially since the appearance of Klausmeier's deterministic model for striped vegetation patterns based on competition for water in [13]. Further developments have focused on vegetation pattern formation models which include additional variables such as surface water, soil moisture, species competition, and plant density, etc., see for instance [18, 24–26].

The effects of random fluctuations on several environmental models have also been vastly studied [21] as the cause of (dis)appearing characteristics in deterministic models, a phenomenon known as *noise-induced transitions*, [12]. More recently, the effects of noise on dryland ecosystems that are usually described by deterministic models showing bistability has been largely studied [18, 21]. Results have emphasized the possibility of noise-induced creation of vegetation patterns, as well as the complete disappearance of vegetated states. For example, Meron and Gilad [18] explain that desertification, the (often) irreversible transition from a vegetated to a bare-soil state, is an example of a naturally occurring phenomena known as hysteresis. In this case, the vegetated state lost to drought is not easily recovered once precipitation levels return to normal, because the bare-soil state is stable. An excess of rainfall is thus necessary to restore the vegetation.

Following the ideas in [14, 16, 17], we begin with a microscopic individual-based model (IBM) that incorporates the interactions occurring in a highly idealized water-vegetation system. The model involves only water and vegetation biomass interactions, with individuals living in an environment of limited capacity. When this capacity, or "system size", increases without bound, the reaction part of Klausmeier's deterministic system emerges (the macroscopic model). We then derive an intermediate mesoscale stochastic model which lies between the individual-based microscale model and that of Klausmeier's deterministic model. Using his estimated parameters for vegetation and precipitation in semi-arid landscapes, and data for state precipitation anomalies in California as baseline, we estimate the mean times for a system to reach the bare-soil "desert" state in a range of realistic precipitation anomalies (departures from long term mean), under the assumption that the precipitation distribution trends do not change in time. With these results we finally quantify, for this simplified model, the dependence between changes in precipitation anomalies and mean time to reach the bare-soil state.

We conclude this chapter with an overview of the Klausmeier model for vegetation-water systems. Drawing on his work, and using his estimates for various parameter values, we derive the mesoscale model in Chapter 2. Chapter 3 details the simulations produced

by the model and Chapter 4 contains our conclusions and suggestions for further study.

1.2 Klausmeier's Model for Vegetation Patterns

C.A. Klausmeier introduced in [13] a deterministic model that produces spatial patterns with the same characteristics of those observed in semiarid vegetation systems. In his model, vegetation growth and water supply are related through the following system of partial differential equations

$$\begin{aligned}\partial_T W &= \underbrace{A}_{\text{water supply}} - \underbrace{LW}_{\text{water evaporation}} - \underbrace{RG(W)F(P)P}_{\text{water consumed by plants}} + \underbrace{V\partial_X W}_{\text{water advection}} \\ \partial_T P &= \underbrace{JRG(W)F(P)P}_{\text{biomass increase}} - \underbrace{MP}_{\text{vegetation death}} + \underbrace{D\Delta P}_{\text{vegetation diffusion}} ,\end{aligned}$$

where W and P represent water and plant biomass densities respectively. The model is set up in a two-dimensional domain with no boundaries. In the original paper Klausmeier simplified the model by taking $G(W) = W$ and $F(P) = P$, which results in the equations

$$\begin{aligned}\partial_T W &= A - LW - RWP^2 + V\frac{\partial W}{\partial X} \\ \partial_T P &= JRWP^2 - MP + D\left(\frac{\partial^2}{\partial X^2} + \frac{\partial^2}{\partial Y^2}\right)P .\end{aligned}$$

To reduce the number of parameters, the model can be nondimensionalized by rescaling as follows:

$$\begin{aligned} w &= JW\frac{R^{\frac{1}{2}}}{L^{\frac{1}{2}}} & p &= P\frac{R^{\frac{1}{2}}}{L^{\frac{1}{2}}} & \hat{m} &= \frac{M}{L} & a &= J\frac{AR^{\frac{1}{2}}}{L^{\frac{3}{2}}} \\ v &= \frac{V}{L^{\frac{1}{2}}D^{\frac{1}{2}}} & t &= LT & x &= X\frac{L^{\frac{1}{2}}}{D^{\frac{1}{2}}} & y &= Y\frac{L^{\frac{1}{2}}}{D^{\frac{1}{2}}} .\end{aligned}$$

These rescalings are from [13], though I have used different notation. Note that rescaling the model without including the spatial terms results in the same variables as scaling with the spatial terms (see Appendix A). Thus the dimensionless system is reduced to a system with only three parameters: a which regulates water input, $\hat{m}$ which refers to vegetation

loss, and v which controls the velocity of the water as it flows downhill:

$$\begin{aligned} \frac{\partial w}{\partial t} &= a - w - wp^2 + v\frac{\partial w}{\partial x} \\ \frac{\partial p}{\partial t} &= wp^2 - \hat{m}p + \frac{\partial^2 p}{\partial x^2} + \frac{\partial^2 p}{\partial y^2}\,. \end{aligned} \tag{1.1}$$

The consideration of advection and diffusion in the model creates an instability that generates a pattern of stripes. In contrast with Turing instability, the determining eigenvalue has negative imaginary part, [22].

1.2.1 Equilibria

Notice that when $p = 0$, $w = a$. Thus the point $(a, 0)$ is an equilibrium point. Linearization of the system at this point shows that $(a, 0)$ is a stable spiral. This makes sense intuitively, since $p = 0$ corresponds to the state where there is no vegetation. Thus, this equilibrium always exists and is stable.

To find the other equilibria we examine the nullclines. When $\frac{dp}{dt} = 0$, $p = \frac{\hat{m}}{w}$. When $\frac{dw}{dt} = 0$, $p = \sqrt{\frac{a}{w} - 1}$. Setting these two p values equal to each other gives $w = \frac{a+\sqrt{a^2-4\hat{m}^2}}{2}$ and $w = \frac{a-\sqrt{a^2-4\hat{m}^2}}{2}$. Thus we have two equilibria at the points $(w_1^*, p_1^*) = (\frac{a+\sqrt{a^2-4\hat{m}^2}}{2}, \frac{2\hat{m}}{a+\sqrt{a^2-4\hat{m}^2}})$ and $(w_2^*, p_2^*) = (\frac{a-\sqrt{a^2-4\hat{m}^2}}{2}, \frac{2\hat{m}}{a-\sqrt{a^2-4\hat{m}^2}})$, so long as $a > 2\hat{m}$. The nullclines indicate one of these is stable while the other is unstable (see Figure 1.1). The linearization of these points shows that the latter is stable. Evaluating the Jacobian of this system at the point (w_2^*, p_2^*):

$$J = \left[\begin{array}{cc} -1 - p^2 & -2wp \\ p^2 & 2wp - \hat{m} \end{array}\right]_{(p_2^*, w_2^*)} = \left[\begin{array}{cc} -1 - \frac{2\hat{m}^2}{a^2 - a\sqrt{a^2-4\hat{m}^2} - 2\hat{m}^2} & -2\hat{m} \\ \frac{2\hat{m}^2}{a^2 - a\sqrt{a^2-4\hat{m}^2} - 2\hat{m}^2} & \hat{m} \end{array}\right],$$

yields a determinant which is positive and a trace which is negative for $a > 2\hat{m}$:

$$\begin{aligned} Det &= -\hat{m} + \frac{2\hat{m}^3}{a^2 - a\sqrt{a^2 - 4\hat{m}^2} - 2\hat{m}^2} \\ T &= \hat{m} - 1 - \frac{2\hat{m}}{a^2 - a\sqrt{a^2 - 4\hat{m}^2} - 2\hat{m}^2}\,. \end{aligned}$$

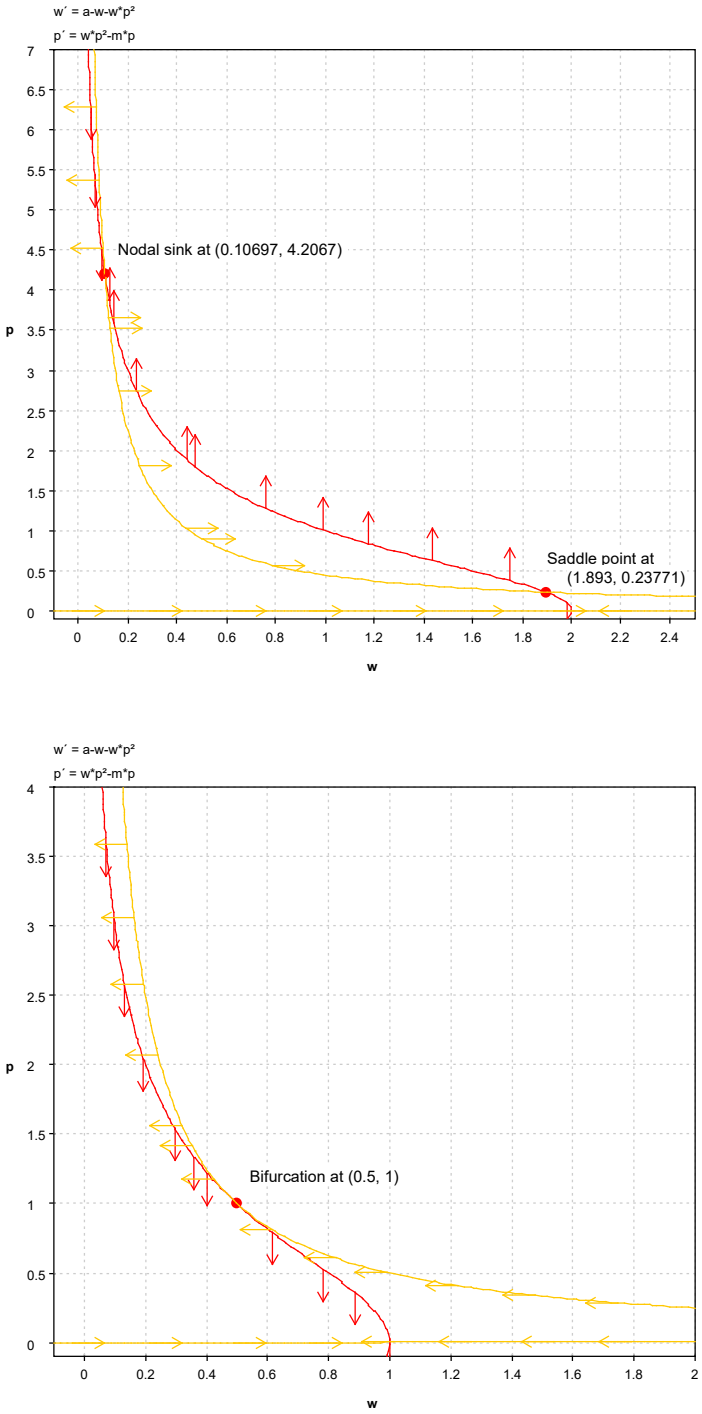

Fig. 1.1: Nullclines and equilibrium points (top) of Klausmeier's non-spatial model with parameter values $a = 2, m = 0.45$. The bifurcation point at $a = 2m$ is shown in the bottom chart. Parameter values $a = 1, m = 0.5$.

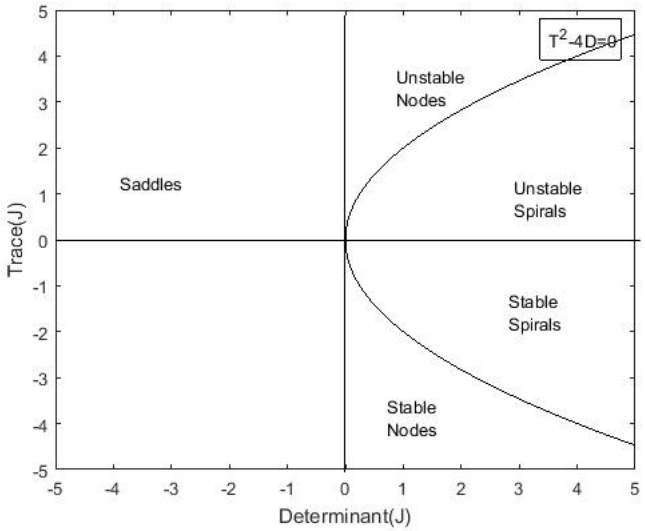

Fig. 1.2: Stability of a two-dimensional fixed point based on the determinant and trace of the Jacobian matrix.

Thus it is easy to see that (w_2^*, p_2^*) is a stable steady state. (See Figure 1.2.)

CHAPTER 2

THEORETICAL FRAMEWORK

The so called *mesoscale* description for a system is an intermediate approximation that emerges between the individual probabilistic model (microscopic IBM description) and the equations for the mean-field (macroscopic description). At the mesoscale approximation the state variables are assumed continuous but the effects of random fluctuations are not lost. In other words, the equations include mean field terms and terms which express random fluctuations around the mean. We derive the mesoscale description of our model by first building the IBM. Along the way we will also make contact with the macroscopic description.

2.1 The Individual-Based Model

We follow the "patch model" introduced by McKane in [16] to write an individual-based model (IBM) that incorporates the main events observed in a vegetation-water system as described by Klausmeier. A patch may be thought of as a small spatial region within which individual elements can interact. We first consider a patch which is small enough that there are no spatial effects; all individuals have the same chance of interacting with each other. For our purposes we assume a patch which has finite capacity, say N, containing the following three elements.

B: vegetation biomass unit

W: water volume unit

E: empty location

Notice that we consider an empty location as an "element". This corresponds with an empty space in a spatial model; however, in a spatial model we would need to define how

each of the individuals (including empty spaces) interact with each other. In this non-spatial version, however, we assume that there is complete mixing, that is, that any two individuals randomly chosen from the patch have as much chance of interacting as any other two random individuals from the patch.

2.1.1 Plant Biomass and Water Dynamics

The dynamics of plant biomass and water interactions are driven by events involving one or two individuals:

$$\begin{aligned} B &\xrightarrow{d} E \\ E &\xrightarrow{s} W \\ W &\xrightarrow{v} E \\ BW &\xrightarrow{b} BB \\ WB &\xrightarrow{b} BB \end{aligned} \tag{2.1}$$

These interactions describe (in order): (i) vegetation biomass loss, (ii) incoming water, (iii) water evaporation, (iv and v) increase in vegetation biomass through water absorption. The corresponding rates at which the interactions occur are given by d, s, v, and b, respectively. The events are assumed to be independent and without memory: they are not influenced by any previous states of the system.

Let us assume that initially there are n elements of type B, m elements of type W and $N - n - m$ elements of type E. Then the probability of randomly choosing the various combinations from the patch are:

probability of drawing $B = \frac{n}{N}$

probability of drawing $W = \frac{m}{N}$

probability of drawing $E = \frac{N-n-m}{N}$

probability of drawing $BW = 2\frac{n}{N}\frac{m}{N-1}$.

We multiply the last combination by a factor of 2 because the choices BW and WB are the same. We can now use these results to determine the transition rates for each event in equations (2.1).

2.1.2 Probability Transition Rates

The transition probability from a state with n plant (B) individuals and m water (W) individuals, that is, from a state (n, m) to (n', m') individuals, in one unit time step, is denoted by $T(n', m'|n, m)$. Notice that it is only possible for transitions from $n \pm 1$ and $m \pm 1$ to take place during each time step. Since we only list the transitions that are involved in the interaction, the only nonzero probability rates in our model are characterized by:

$$\begin{aligned} T(n+1, m-1|n, m) &= 2b\frac{n}{N}\frac{m}{N-1} \\ T(n-1, m|n, m) &= d\frac{n}{N} \\ T(n, m+1|n, m) &= s\frac{N-n-m}{N} \\ T(n, m-1|n, m) &= v\frac{m}{N}\,. \end{aligned} \tag{2.2}$$

2.1.3 The Kolmogorov Equation

The probability of having n, m individuals in the patch at time t is given by the probability density function $P(n, m, t)$. This probability changes with time, and the rate of change of this function with respect to time is simply the sum of the transitions into the state with n, m individuals minus the sum of the transitions out of the state with n, m individuals. Thus we can write the following differential equation, also known as the

Kolmogorov equation:

$$\begin{aligned}\frac{dP(n,m,t)}{dt} &= T(n,m|n-1,m+1)P(n-1,m+1,t) + T(n,m|n+1,m)P(n+1,m,t) \\ &+T(n,m|n,m+1)P(n,m+1,t) + T(n,m|n,m-1)P(n,m-1,t) \\ &- [T(n+1,m-1|n,m) + T(n-1,m|n,m) + T(n,m-1|n,m) \\ &+ T(n,m+1|n,m)]\, P(n,m,t)\,.\end{aligned} \tag{2.3}$$

The boundary values $n, m = 0$ and $n, m = N$ (the smallest and largest number of elements in the patch, respectively) imply the following transition probabilities at the boundaries:

$$\begin{aligned} T(-1,m|0,m) &= 0 \\ T(n,-1|n,0) &= 0 \\ T(N+1,m|N,m) &= 0 \\ T(n,N+1|n,N) &= 0\,. \end{aligned}$$

The following transitions are also zero according to our equations (2.2) for the transition rates:

$$\begin{aligned} T(0,m|-1,m) &= 0 \\ T(n,0|n,-1) &= 0 \\ T(N,m|N+1,m) &= 0 \\ T(n,N|n,N+1) &= 0\,. \end{aligned}$$

Thus, given an initial condition $P(n,m,0)$, equation 2.3 completely describes the evolution in time of the state of the system. This is the microscopic model description of the system.

2.2 The Mean-Field Equations

We can write the expression for the rate of change of the average value over the system, $\frac{d\langle n\rangle}{dt}$ (angled brackets denote the average value) by multiplying $\frac{dP(n,m,t)}{dt}$ by n and summing over m and n. Note that none of the transition probabilities involving changes only in m will enter into the equation for $\frac{d\langle n\rangle}{dt}$, and vice versa. Thus:

$$\begin{aligned}\frac{d}{dt}\sum_{n,m=0}^{N} nP(n,m,t) = \sum_{n,m=0}^{N} n\ [&T(n,m|n-1,m+1)P(n-1,m+1,t)\\ &+T(n,m|n+1,m)P(n+1,m,t)\\ &+T(n,m|n,m+1)P(n,m+1,t)\\ &+T(n,m|n,m-1)P(n,m+1,t)\\ &-T(n+1,m-1|n,m)P(n,m,t)\\ &-T(n-1,m|n,m)P(n,m,t)\\ &-T(n,m-1|n,m)P(n,m,t)\\ &-T(n,m+1|n,m)P(n,m,t)]\,.\end{aligned}$$

By shifting the variable in two of the sums on n and m by ± 1, and by shifting m by -2 in the first sum,we obtain:

$$\begin{aligned}\frac{d\langle n\rangle}{dt} = \sum_{m=0}^{N}\sum_{n=0}^{N}&(n+1)T(n+1,m-1|n,m)P(n,m,t)\\ &+(n-1)T(n-1,m|n,m)P(n,m,t)\\ &+nT(n,m-1|n,m)P(n,m,t)\\ &+nT(n,m+1|n,m)P(n,m,t)\\ &-nT(n+1,m-1|n,m)P(n,m,t)\\ &-nT(n-1,m|n,m)P(n,m,t)\\ &-nT(n,m-1|n,m)P(n,m,t)\\ &-nT(n,m+1|n,m)P(n,m,t)\,,\end{aligned}$$

which reduces to:

$$\frac{d\langle n\rangle}{dt} = \sum_{n,m=0}^{N} \left[T(n+1,m-1|n,m) - T(n-1,m|n,m)\right] P(n,m,t)\,.$$

Sustituting expressions for the transition rates (2.2) gives:

$$\frac{d\langle n\rangle}{dt} = 2b\frac{\langle n\rangle}{N}\frac{\langle m\rangle}{N-1} - d\frac{\langle n\rangle}{N}\,. \tag{2.4}$$

Similarly,

$$\begin{aligned}
\frac{d}{dt}\sum_{n,m=0}^{N} mP(n,m,t) = \sum_{n,m=0}^{N} m\ [&T(n,m|n-1,m+1)P(n-1,m+1,t)\\
&+ T(n,m|n+1,m)P(n+1,m,t)\\
&+ T(n,m|n,m+1)P(n,m+1,t)\\
&+ T(n,m|n,m-1)P(n,m+1,t)\\
&- T(n+1,m-1|n,m)P(n,m,t)\\
&- T(n-1,m|n,m)P(n,m,t)\\
&- T(n,m-1|n,m)P(n,m,t)\\
&- T(n,m+1|n,m)P(n,m,t)]\\
&= \sum_{n=0}^{N}\sum_{m=0}^{N}(m-1)T(n+1,m-1|n,m)P(n,m,t)\\
&+ mT(n-1,m|n,m)P(n,m,t)\\
&+ (m-1)T(n,m-1|n,m)P(n,m,t)\\
&+ (m+1)T(n,m+1|n,m)P(n,m,t)\\
&- mT(n+1,m-1|n,m)P(n,m,t)\\
&- mT(n-1,m|n,m)P(n,m,t)\\
&- mT(n,m-1|n,m)P(n,m,t)\\
&- mT(n,m+1|n,m)P(n,m,t)\,,
\end{aligned}$$

reduces to:

$$\begin{aligned}\frac{d\langle m\rangle}{dt} &= \sum_{n,m=0}^{N}(-1)T(n+1,m-1|n,m)P(n,m,t)\\ &+(-1)T(n,m-1|n,m)P(n,m,t)\\ &+T(n,m+1|n,m)P(n,m,t)\\ &=\sum_{n,m=0}^{N}\left[T(n,m+1|n,m)-T(n,m-1|n,m)-T(n+1,m-1|n,m)\right]P(n,m,t)\,.\end{aligned}$$

Substituting the transition probabilities we have:

$$\frac{d\langle m\rangle}{dt} = s\frac{\langle N-n-m\rangle}{N} - v\frac{\langle m\rangle}{N} - 2b\frac{\langle n\rangle}{N}\frac{\langle m\rangle}{N-1}\,. \tag{2.5}$$

Assuming that N is relatively much larger than $\langle n\rangle$ and $\langle m\rangle$, i.e. $\frac{\langle N-n-m\rangle}{N}$ is close to one, suggests the approximation

$$\frac{d\langle m\rangle}{dt} = s - v\frac{\langle m\rangle}{N} - 2b\frac{\langle n\rangle}{N}\frac{\langle m\rangle}{N-1}\,. \tag{2.6}$$

We remark at this point that water infiltration in the soil is improved by the presence of vegetation; as a consequence, the process of water absorption by plants becomes more efficient [18]. This fact is incorporated into the model by assuming that such improvement is proportional to the vegetation density actually present. In our model, this is equivalent to modifying the transition rate for water absorption and the subsequent increase in vegetation as follows,

$$BW \xrightarrow{bn/N} BB, \quad WB \xrightarrow{bn/N} BB\,.$$

This in turn affects the first transition rate in (2.2), which now becomes

$$T(n+1,m-1|n,m) = 2b\frac{n^2}{N^2}\frac{m}{N-1}\,.$$

When this transition rate is substituted into the equation for $d\langle n\rangle/dt$, it produces

$$\frac{d\langle n\rangle}{dt} = 2b\frac{\langle n^2\rangle}{N^2}\frac{\langle m\rangle}{N-1} - d\frac{\langle n\rangle}{N} \tag{2.7}$$

instead of equation (2.4). A similar change happens in equation (2.6):

$$\frac{d\langle m\rangle}{dt} = s - v\frac{\langle m\rangle}{N} - 2b\frac{\langle n^2\rangle}{N^2}\frac{\langle m\rangle}{N-1}\,. \tag{2.8}$$

Thus, going back to the differential equations for $\langle n\rangle$ and $\langle m\rangle$, we see that Klausmeier's (non-spatial) model is recovered:

$$\begin{aligned}\frac{d\langle n\rangle}{dt} &= \tilde{b}\langle n^2\rangle\langle m\rangle - \tilde{d}\langle n\rangle \\ \frac{d\langle m\rangle}{dt} &= s - \tilde{v}\langle m\rangle - \tilde{b}\langle n^2\rangle\langle m\rangle\ ,\end{aligned} \tag{2.9}$$

where $\tilde{b} = 2b/N^2(N-1)$, $\tilde{d} = d/N$, and $\tilde{v} = v/N$. Equations (2.9) constitute the *mean field* equations for our stochastic water-vegetation system.

2.3 The Continuous Model

Dividing equations (2.7) and (2.5) by N and taking the limit allows us to replace $\langle n^2\rangle$ with $\langle n\rangle^2$. Defining $\phi_n = \langle n\rangle/N$ and $\phi_m = \langle m\rangle/N$ we obtain

$$\begin{aligned}\frac{d\phi_n}{dt} &= \tilde{b}\phi_n^2\phi_m - \tilde{d}\phi_n \\ \frac{d\phi_m}{dt} &= \tilde{s}(1-\phi_n-\phi_m) - \tilde{v}\phi_m - \tilde{b}\phi_n^2\phi_m\,,\end{aligned} \tag{2.10}$$

where now $\tilde{b} = 2b/(N-1)$, $\tilde{d} = d/N$, $\tilde{s} = s/N$, and $\tilde{v} = v/N$. Notice that here $\phi_n(t)$ is the density of vegetation biomass in the given region, thus equations (2.10) are the mean field equations for the density of our stochastic water-vegetation system. Again, the assumption that N is relatively much larger than $\langle n\rangle$ and $\langle m\rangle$, means that the quantity $(1-\phi_n-\phi_m) \approx 1$ which yields the equation

$$\frac{d\phi_m}{dt} = \tilde{s} - \tilde{v}\phi_m - \tilde{b}\phi_n^2\phi_m\,. \tag{2.11}$$

Thus we see that the non-spatial part of Klausmeier's model is recovered.

2.3.1 Numerical Simulations

The IBM can be simulated using a numerical scheme [5] to produce a time series for the number of individuals (vegetation or water), with statistics determined by the probability density function Kolmogorov equation. To do so, we must first determine the transition rates for the stochastic model by identifying the corresponding coefficients in the mean-field approximation (2.9) with those in Klausmeier's nondimensional, nonspatial model (1.1). Accordingly,

$$\begin{aligned} \tilde{b} = 1 \quad &\rightarrow \quad b = \frac{N^2(N-1)}{2} \\ \tilde{d} = \hat{m} \quad &\rightarrow \quad d = \hat{m}N \\ \tilde{v} = 1 \quad &\rightarrow \quad v = N \\ s = a\,. & \end{aligned}$$

Substituting these rates into the transition probabilities yields

$$\begin{aligned} T(n+1, m-1|n, m) &= 2b\frac{n}{N}\frac{m}{N-1} = n^2 m \\ T(n-1, m|n, m) &= d\frac{n}{N} = \hat{m}n \\ T(n, m+1|n, m) &= s\frac{N-n-m}{N} = a \\ T(n, m-1|n, m) &= v\frac{m}{N} = m\,. \end{aligned} \tag{2.12}$$

The results of our simulation are given in Figure 2.1, where we have plotted one stochastic model solution against the mean-field solution. Notice that the stochastic solution fluctuates around the mean-field solution but follows its average behavior over time. These fluctuations represent the intrinsic noise due to the interactions between individuals, rather than external noise such as from the environment. Notice that in the macroscopic description this intrinsic noise is lost. It is for this reason we wish to develop a mesoscale, or intermediate description, in order to retain the stochastic effects caused by the discreteness

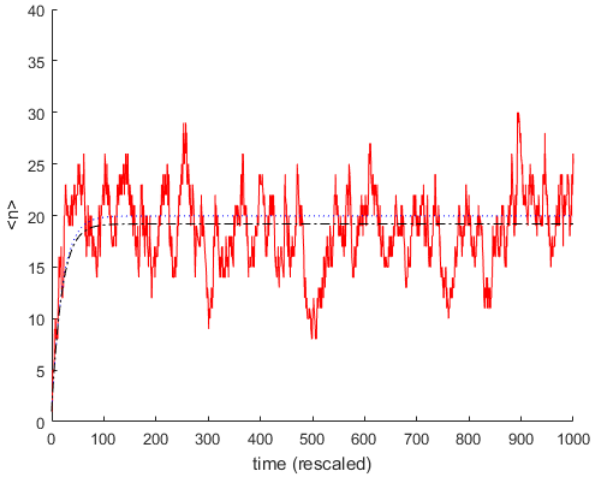

Fig. 2.1: Solution of one stochastic simulation (red, results for vegetation only presented) with the corresponding mean-field dynamics (black dash-dot), plotted against Klausmeier's model (dotted blue line). The equilibrium for Klausmeier's system is $(p^*, w^*) = (19.9499, 0.0501)$. Parameter values: $a = 1$, $\hat{m} = 0.05$ and $N = 500$.

of the individual interactions, as well as the deterministic behavior of the macroscopic level of the system.

2.4 The Mesoscale Approximation

To find the mesoscale model we follow the ideas and notation used in [17], first writing the associated Fokker-Planck (forward Kolmogorov) equation for the stochastic model in section 2.1.3, and then deriving the corresponding stochastic differential equation. We denote with f_i the model transition rates in the limit, $f_i(\phi) = \lim_{N\to\infty} T_i(N\phi + \boldsymbol{\nu}_i | N\phi)$, where the index i has been assigned to the transition rate T according to the enumeration made in section 2.2. The vector $\boldsymbol{\nu}_i$ provides the changes associated with each of the transitions, see Table 2.1.

Table 2.1: Transition rates and associated changes.

index i	1	2	3	4
f_i	$\tilde{b}\phi_n^2\phi_m$	$\tilde{d}\phi_n$	$\tilde{s}(1-\phi_n-\phi_m)$	$\tilde{v}\phi_m$
ν_{ni}	1	-1	0	0
ν_{mi}	-1	0	1	-1

For ease in notation let us write $\phi = (\phi_n, \phi_m)$. Then the associated Fokker-Planck equation reads

$$\begin{aligned}\frac{\partial P(\phi,\tau)}{\partial \tau} = &-\left[\frac{\partial}{\partial \phi_n}\left(A_n(\phi)P(\phi,\tau)\right) + \frac{\partial}{\partial \phi_m}\left(A_m(\phi)P(\phi,\tau)\right)\right] \\ &+ \frac{1}{2N}\left[\frac{\partial^2}{\partial \phi_n^2}\left(B_{nn}(\phi)P(\phi,\tau)\right) + 2\frac{\partial^2}{\partial \phi_n \partial \phi_m}\left(B_{nm}(\phi)P(\phi,\tau)\right)\right. \\ &\left. + \frac{\partial^2}{\partial \phi_m^2}\left(B_{mm}(\phi)P(\phi,\tau)\right)\right],\end{aligned} \tag{2.13}$$

where

$$\begin{aligned}A_n(\phi) &= \tilde{b}\phi_n^2\phi_m - \tilde{d}\phi_n \\ A_m(\phi) &= S(1-\phi_n-\phi_m) - \tilde{b}\phi_n^2\phi_m - \tilde{v}\phi_m \\ B_{nn}(\phi) &= \tilde{b}\phi_n^2\phi_m + \tilde{d}\phi_n \\ B_{nm}(\phi) &= B_{mn}(\phi) = -\tilde{b}\phi_n^2\phi_m \\ B_{mm}(\phi) &= \tilde{b}\phi_n^2\phi_m + S(1-\phi_n-\phi_m) + \tilde{v}\phi_m\end{aligned}$$

and where time has been rescaled to $\tau = t/N$. If we denote B with the symmetric matrix

$$B = \begin{bmatrix} B_{nn} & B_{nm} \\ B_{mn} & B_{mm} \end{bmatrix}$$

then the associated stochastic differential equations system associated with the Fokker-Planck equation above is given by

$$\begin{aligned} d\phi_n &= A_n(\phi)d\tau + \frac{1}{\sqrt{N}} g_{nn}(\phi) dW_1, \\ d\phi_m &= A_m(\phi)d\tau + \frac{1}{\sqrt{N}} \left[g_{mn}(\phi) dW_1 + g_{mm}(\phi) dW_2 \right] , \end{aligned} \tag{2.14}$$

where the g's are the function elements in the matrix decomposition of B as the product gg^T, with

$$\begin{aligned} g &= \begin{bmatrix} g_{nn} & 0 \\ g_{mn} & g_{mm} \end{bmatrix} \\ &= \begin{bmatrix} \sqrt{\tilde{b}\phi_n^2\phi_m + \tilde{d}\phi_n} & 0 \\ -\tilde{b}\phi_n^2\phi_m / \sqrt{\tilde{b}\phi_n^2\phi_m + \tilde{d}\phi_n} & \sqrt{\tilde{b}\phi_n^2\phi_m + S(1-\phi_n-\phi_m) + \tilde{v}\phi_m - \frac{(\tilde{b}\phi_n^2\phi_m)^2}{\tilde{b}\phi_n^2\phi_m + \tilde{d}\phi_n}} \end{bmatrix}. \end{aligned}$$

The procedure of going from a Fokker-Planck equation like (2.13) to the stochastic system in equations (2.14) can be found, for instance, in [8].

CHAPTER 3

SIMULATIONS

We use the stochastic differential equations (2.14) to numerically simulate the water-vegetation system and obtain averages of the expected time of absorption into the bare-soil state, subject to negative average precipitation anomalies, [11].

First, we identify the parameters of the non-dimensional deterministic (non-spatial) model in Klausmeier's paper [13] with the mean field system obtained above ($A_n(\phi)$ and $A_m(\phi)$). We find that $S = AR^{\frac{1}{2}}J/L^{\frac{3}{2}}$ and $\tilde{d} = M/L$. The meaning and realistic values for these parameters are listed in Table 3.1. Thus, for instance, Klausmeier's parameter ranges for trees are $S = 0.077$ to 0.23 and $\tilde{d} = 0.045$, and for grass they are $S = 0.94$ to 2.81 and $\tilde{d} = 0.45$. Also, the corresponding value for $\tilde{b}$ and $\tilde{v}$ in both cases is one. Regarding the average evaporation rate, we follow Klausmeier in assuming that the equilibrium of water (in his deterministic model) is at $w^* = 75$ kg H_2O m^{-2}, and then computing the associated evaporation rate given the averaged annual precipitation, [13]. For example, with $A = 300$ kg H_2O $m^{-2}year^{-1}$ the evaporation rate is $L = A/w^* = 4$ $year^{-1}$.

Table 3.1: Parameters for semi-arid landscapes, [13].

R	uptake rate of water	1.5 (trees) or 100 (grass)	kg H_2O $m^{-2}year^{-1}$ (kg dry mass)$^{-2}$
J	yield of plant biomass	0.002 (trees) or 0.003 (grass)	kg dry mass (kg H_2O)$^{-1}$
M	mortality rate	0.18 (trees) or 1.8 (grass)	$year^{-1}$
A	precipitation	250-750	kg H_2O $m^{-2}year^{-1}$
L	evaporation rate	4	$year^{-1}$

Second, public records in precipitation anomalies (changes in long term average) suggest a trend of negative values in specific geographic locations. In the state of California, for example, the state average of the anomalies for the past 16 years is ≈ -2.07 inches $year^{-1}$ (-52.58 kg H_2O $m^{-2}year^{-1}$) (see Figure 3.1). Although there is a lot of variability across the state, we use this value only for illustration purposes, and similarly assume that this

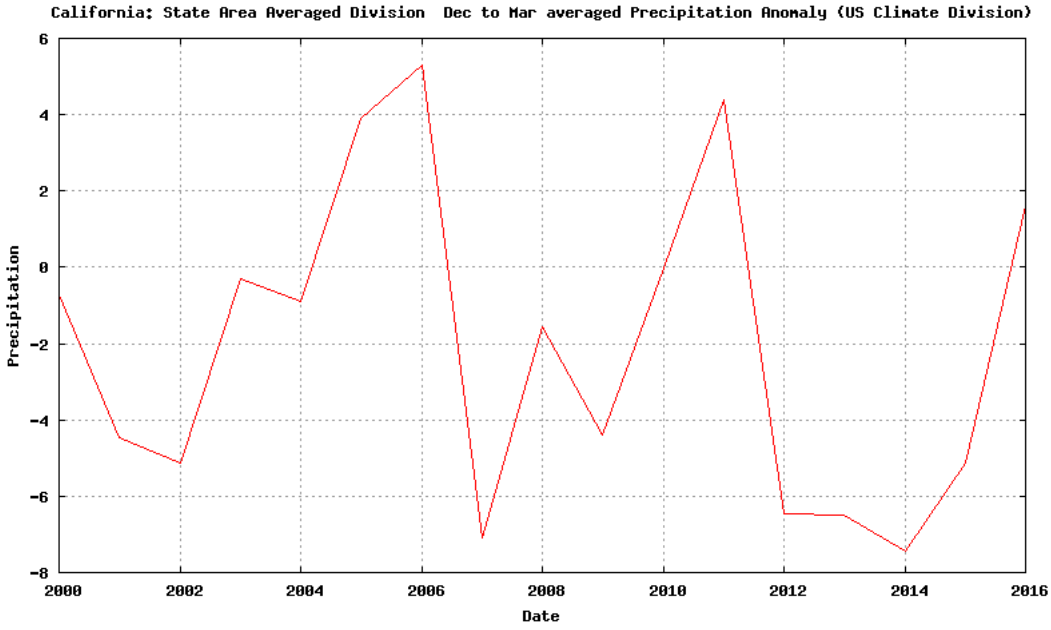

Fig. 3.1: State averages of precipitation anomalies for 2000-2016 in California (inches year^{-1}). The averaged anomaly (difference from long term average) during that period is ≈ -2.07 inches year^{-1} (-52.48 kg H_2O m^{-2}year^{-1}). The precipitation increase expected from El Niño for the winter 2015-2016 was scarcely above the long term state average. Data/image provided by the NOAA/OAR/ESRL PSD, Boulder, Colorado, USA, from their Web site at http://www.esrl.noaa.gov/psd.

negative deviation from the precipitation average is steady in time.

The results from the simulations are shown in Figure 3.2, portraying a rough linear relation between the time to absorption into the bare-soil state and the anomalies in precipitation in the range selected. The simulations were run using parameters for trees and grass, with system capacity $N = 500$.

We are interested in identifying how negative changes in precipitation affect the time to desertification. In other words, how sensitive is the average time to absorption into the bare-soil state to small perturbations in precipitation? In order to do this we define the (dimensionless) sensitivity index S_0 as the ratio $S_0 = (\Delta T/T)/(\Delta P/P)$, where T is the average time to absorption, P is the average annual precipitation, and ΔT and ΔP represent the absolute change in T and P, respectively (see for instance [2, 3]). Direct computation from the averaged results gives $S_0 \approx 2$. Similar results were obtained with

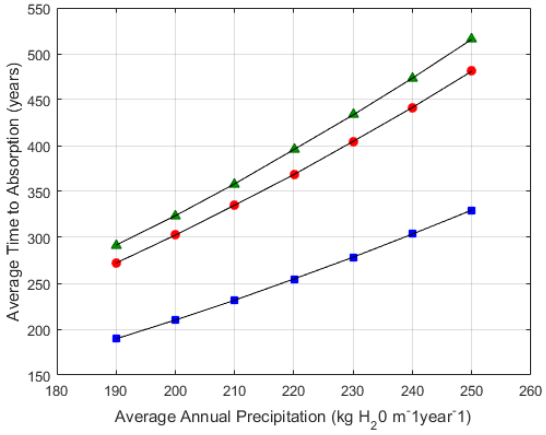

(a) Trees

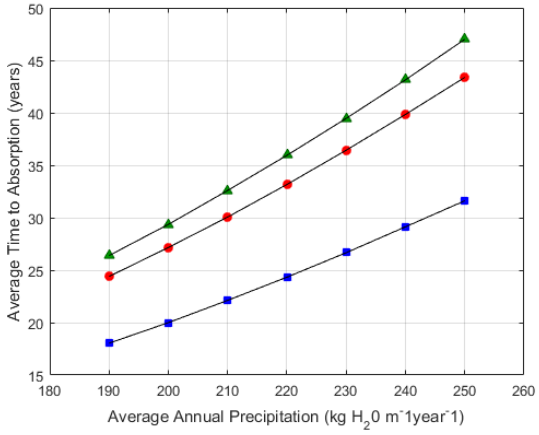

(b) Grass

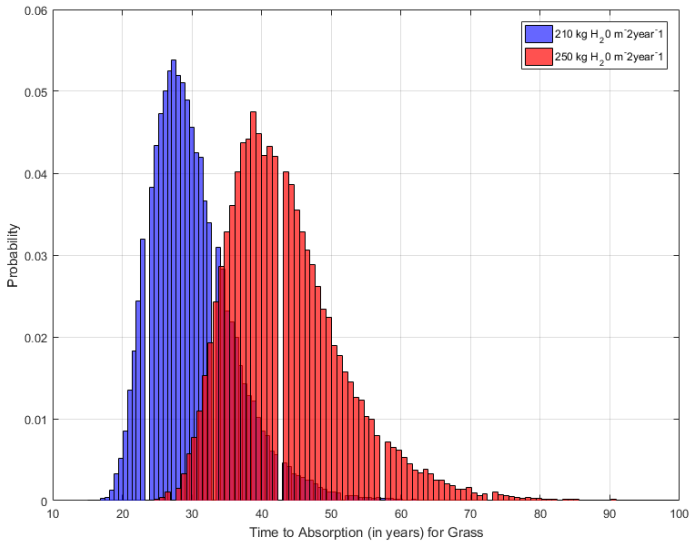

(c)

Fig. 3.2: Examples of how average time to absorption into the bare-soil state might be affected by a reduction in average annual precipitation. Parameters for trees were used in panel (a) and for grass in panel (b). The average of negative anomalies similar to that observed for the last years in California is around $\approx$ 50 kg H_20 $m^{-2}year^{-1}$. The model suggests that the sensitivity index $S_0 \approx 2$, that is, relative changes in the mean time to absorption are roughly twice the relative changes in average annual precipitation. For the simulations, $N = 500$ and the initial conditions were $\phi(0) = (0.1, 0.1)$ (squares), $\phi(0) = (0.5, 0.5)$ (circles), and $\phi(0) = (0.9, 0.1)$ (triangles). Each time average was obtained from $50,000$ simulations. Simulations using $N = 10^4$ (see Figure D.1 in Appendix D) gave the same approximate value of S_0. Panel (c) shows the histograms corresponding to the simulated times of absorption with an average annual precipitation of 210 (left/blue) and 250 (right/red) kg H_20 $m^{-2}year^{-1}$ for grass. The simulations used the same system capacity, $N = 500$, and initial conditions $\phi(0) = (0.5, 0.5)$.

Table 3.2: Sensitivity Index values $S_0 = (\Delta T/T)/(\Delta P/P)$ for $N = 500$ and $N = 10^4$ for grass with initial conditions $\phi_0 = (0.1, 0.1)$ and for trees with initial conditions $\phi_0 = (0.5, 0.5)$.

	Grass		**Trees**	
$\boldsymbol{\Delta P}$	$N = 500$	$N = 10^4$	$N = 500$	$N = 10^4$
$250 - 240$	1.9619	2.0307	2.05	2.046
$240 - 230$	2.0316	2.0267	2.0105	2.0026
$230 - 220$	2.0144	2.0138	2.0537	2.0101
$220 - 210$	1.9966	1.9997	1.9927	2.0217
$210 - 200$	2.0169	2.0371	2.0422	1.9926
$200 - 190$	1.9591	1.9982	2.0129	2.0111

the larger system capacity $N = 10^4$ (see Table 3.2). This implies, for example, that a 2% decrease in precipitation will result in a 4% decrease in the time to desertification.

CHAPTER 4

SUMMARY AND CONCLUSIONS

We have derived a system of stochastic differential equations that describe the dynamics of an idealized water-vegetation system. The model is intermediate between an individual-based and the deterministic model (Klausmeier's reaction part). With realistic parameter values for vegetation and precipitation for semi-arid landscapes, and current data on drought trends in California as example, we computed average times for the transition from a vegetated state to bare-soil (see Figures 3.2 and D.1). For a fixed system capacity ($N = 500$) the simulations for trees and grass suggest that the sensitivity of the time to absorption into the bare-soil state to change in the annual precipitation is roughly similar and approximately equal to 2. Repeating the simulations, first for different initial conditions and then for a larger capacity ($N = 10^4$), provided the same approximate relation.

The model suggests that a 4% decrease in precipitation will result in the time to desertification being shortened by roughly 8%. For example, a decrease of 0.4 inches of precipitation (10 kg H_2O $m^{-2}year^{-1}$) might reduce time to absorption into the bare-soil state by more than 25 years for the case of trees, and nearly 5 years in the case of grass (see Figure 3.2). In other words, current trends of desertification could be significantly boosted if the patterns of decreasing precipitation anomalies are maintained. However, looking at the basic transition mechanisms considered here to derive the equations, it is clear that the model should be used with care to draw any conclusions on specific vegetation-water systems. Our model ignored the spatial dynamics of these systems, and simulations using a spatial mesoscale model (see Appendix C) may provide further insight into semi-arid environments and how they respond to changes in precipitation.

We remark that extended droughts may resemble desertification, but the return of seasonal precipitation events may recover the vegetation (see for instance [1, 10], where desertification was limited to localized areas). This suggests that the inclusion of patterns

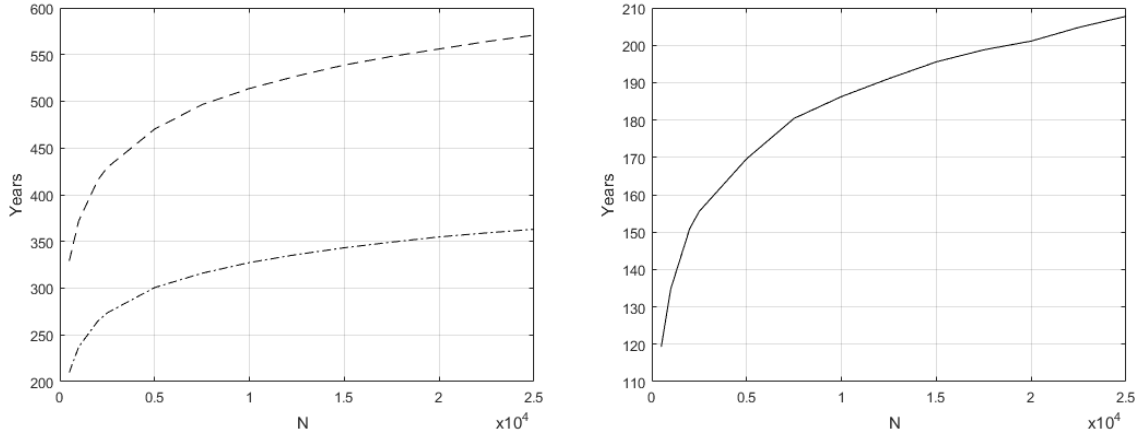

(a) (b)

Fig. 4.1: Time to absorption as a function of the system capacity N. Panel (a) shows time to absorption for two different precipitation values: $A = 250$ (dashes) and $A = 200$ (dot-dashes). The sensitivity of the time to absorption from the annual precipitation computed for $N = 10000$ was the same as when $N = 500$, that is, $S_0 \approx 2$. As N increases, both times to extinction also increase, but they decrease dramatically as N gets smaller. Panel (b) shows the difference between the curves in the contiguous plot. Although the difference increases, the sensitivity of the time to absorption from the annual precipitation is apparently similar in relatively large systems.

of localized precipitation anomalies would provide more reliable results for extinction times. For relatively small systems we notice that the times for absorption into the bare-soil state may be reduced dramatically (see Figure 4.1).

Further work should also include long term variations of other climate related parameters. For instance, it has been documented that higher temperatures increase evapotranspiration rates [4]. In particular, increments in evaporation rates have been observed over most of the United States, with the exception of the Southeast, Northeast and the Great Lake regions, [9]. These increments depend on the location and vary up to 2% every ten years.

BIBLIOGRAPHY

[1] A. Anyamba, C.J. Tucker(2005) Analysis of Sahelian vegetation dynamics using NOAA-AVHRR NDVI data from 1981-2003. Journal of Arid Environments, 63, 596-614.

[2] L. Arriola and J. Hyman, Forward and adjoint sensitivity analysis: with applications in Dynamical Systems, Linear Algebra and Optimization, Lecture Notes, Mathematical and Theoretical Biology Institute, 2005.

[3] L. Arriola, J.M. Hyman. Sensitivity analysis for uncertainty quanitification in mathematical models, in *Mathematical and Statistical Estimation Approaches in Epidemiology* (G. Chowell, J.M. Hyman, L.M.A. Betancourt, D. Bies, editors), Springer, Netherlands, 2009.

[4] B.C. Bates, Z. W. Kundzewicz, S. Wu and J. P. Palutikof, Eds., 2008: Climate Change and Water. Technical Paper of the Intergovernmental Panel on Climate Change, IPCC Secretariat, Geneva, 210 pp.

[5] T. Biancalani, *The Influence of Demographic Stochasticity on Population Dynamics*, Ph.D. thesis, Universtiy of Illinois at Urbana-Champaign, Urbana, IL, 2014.

[6] P. Chesson, R.L.E. Gebauer, S. Schwinning, et al. (2004) Resource pulses, species interactions, and diversity maintenance in arid and semi-arid environments. Oecologia 141:236-253. doi:10.1007/s00442-004-1551-1

[7] J. von Hardenberg, E. Meron, M. Shachak, Y. Zarmi (2001) Diversity of vegetation patterns and desertification. Physical Review Letters, 87, 19, 198101, 1-4.

[8] C. Gardiner, *Handbook of Stochastic Methods for Physics, Chemistry and the Natural Sciences*, 4th ed., Springer, Berlin 2009.

[9] V.S. Golubev, J.H. Lawrimore, P.Y. Groisman, N.A. Speranskaya, S. A. Zhuravin, M.J. Menne, T.C. Peterson, R.W. Malone (2001) Evaporation changes over the contiguous United States and the former USSR: A reassessment. Geophysical Research Letters, 28, 13, 2665-2668.

[10] U. Helldèn (1991) Desertification: Time for assessment?. Ambio, 20, 8, Forestry and the Environment, 372-383.

[11] D.J. Higham (2001) An algorithmic introduction to numerical simulation of stochastic differential equations. SIAM Review, 43, 3, 525-546.

[12] W. Horsthemke, R. Lefever *Noise-Induced Transitions: Theory and Applications in Physics, Chemistry and Biology.* Springer, Berlin, 1984.

[13] C.A. Klausmeier (1999) Regular and irregular patterns in semiarid vegetation. Science, 284, 1826-1828.

[14] C.A. Lugo, A.J. McKane (2008) Quasicycles in a spatial predator-prey model. Physical Review E, 78, 051911.

[15] C.S. Mantyka-Pringle, T.G. Martin, J.R. Rhodes (2012) Interactions between climate and habitat loss effects on biodiversity: a systematic review and meta-analysis. global Change Biology, 18, 1239-1252.

[16] A.J. McKane, T.J. Newman (2004) Stochastic models in population biology and their deterministic analogs. Physical Review E, 70, 041902, 19 pages.

[17] A.J. McKane, T. Biancalini, T. Rogers (2014) Stochastic pattern formation and spontaneous polarization: the linear noise approximation and beyond. Bulletin of Mathematical Biology, 76, 895-921.

[18] E. Meron, E. Gilad. Dynamics of plant communities in drylands: a pattern formation approach. In *Complex Population Dynamics: Nonlinear Modeling in Ecology, Epidemiology and Genetics.* (B. Blasius, J. Kurths, L. Stone, editors), World Scientific, Singapore, 2007, pgs 49-75.

[19] S.E. Nicholson *Dryland Climatology.* Cambridge, GB: Cambridge University Press, 2011.

[20] NOAA National Centers for Environmental Information, State of the Climate: Drought for August 2016, published online September 2016, retrieved on October 5, 2016 from http://www.ncdc.noaa.gov/sotc/drought/201608.

[21] L. Rindolfi, P. D'Ocorico, F. Laio *Noise-Induced Phenomena in the Environmental Sciences.* Cambridge University Press, New York, 2011.

[22] A.B. Rovinsky, M. Mezinger (1992) Chemical instability induced by a differential flow. Physical Review Letters, 69, 8, 1193-1196.

[23] J. Sheffield, E.F. Wood (2008) Global trends and variability in soil moisture and drought characteristics, 1950-2000, from observation-driven simulations of the terrestrial hydrologic cycle. Journal of Climate, 21, 432-458.

[24] J.A. Sherratt (2005) An analysis of vegetation stripe formation in semi-arid landscapes. Journal of Mathematical Biology, 51, 183-197.

[25] J. A. Sherratt, G.J. Lord (2007) Nonlinear dynamics and pattern bifurcations in a model for vegetation stripes in semi-arid environments. Theoretical Population Biology, 71, 1-11.

[26] J.A. Sherratt (2013) Pattern solutions of the Klausmeier model for banded vegetation in semi-arid environments V: the transition from patterns to desert. SIAM Journal of Applied Mathematics, 73, 1347-1367.

APPENDICES

Appendix A

Rescaling Klausmeier's Non-spatial Model

In this appendix we present a rescaling of Klausmeier's non-spatial model. Initially, we ignored the spatial terms in Klausmeier's nondimensionalized equations. The question arose, however, whether rescaling the original equations (with spatial terms included) would result in the same nondimensionalized equations as rescaling the original equations without including their spatial terms. We found that the nondimensionalized equations are the same in either case.

Let $t = \frac{T}{t_c}, w = \frac{W}{w_c}$ and $p = \frac{P}{p_c}$. Then $T = t_c t, W = w_c w$ and $P = p_c p$. Substituting these values into Klausmeier's model without the spatial terms, as shown below,

$$\frac{dW}{dT} = A - LW - RWP^2 \tag{A.1}$$

$$\frac{dP}{dT} = RJWP^2 - MP \tag{A.2}$$

gives:

$$\frac{dw}{dt} = \frac{t_c}{w_c}A - t_c L w - \frac{p_c^2}{t_c}Rwp^2 \tag{A.3}$$

$$\frac{dp}{dt} = t_c w_c p_c RJwp^2 - t_c Mp\,. \tag{A.4}$$

Set $t_c = L^{-1}$, $p_c = \frac{\sqrt{L}}{\sqrt{R}}$, and $w_c = \frac{\sqrt{L}}{J\sqrt{R}}$. Then

$$\frac{dw}{dt} = A\sqrt{R}JL^{-3/2} - w - wp^2 \tag{A.5}$$

$$\frac{dp}{dt} = wp^2 - \frac{M}{L}p\,. \tag{A.6}$$

Now, let a, which controls water input, equal $A\sqrt{R}JL^{-3/2}$ and m, which controls plant mortality, equal ML^{-1}. Then the equations become

$$\frac{dw}{dt} = a - w - wp^2 \tag{A.7}$$

$$\frac{dp}{dt} = wp^2 - mp\,. \tag{A.8}$$

Thus it is easy to see that these are the same equations as Klausmeier's nondimensionalized model when the spatial terms are ignored.

Appendix B

Analysis of the Mean-field Model

Following is the annalysis of the non-spatial stochastic model we derived in Chapter 2:

$$\frac{d\phi_m}{dt} = \tilde{s}(1-\phi_n-\phi_m) - \tilde{v}\phi_m - \tilde{b}\phi_n^2\phi_m \tag{B.1}$$

$$\frac{d\phi_n}{dt} = \tilde{b}\phi_n^2\phi_m - \tilde{d}\phi_n\,. \tag{B.2}$$

To find the equilibrium points, we examine the nullclines. Notice that when we set $\frac{d\phi_m}{dt} = 0$, then either $\phi_n = 0$ or $b\phi_n\phi_m - d = 0$. However, $\phi_n = 0$ is the trivial case, which is of no interest. (In this case, $\phi_m = \frac{s}{s+v}$ and $(\frac{s}{s+v}, 0)$ is the trivial equilibrium point.) Solving the second factor for ϕ_n yields

$$\phi_n = \frac{d}{b\phi_m}\,. \tag{B.3}$$

Now we set $\frac{d\phi_m}{dt}$ equal to 0 and solve for ϕ_n:

$$\begin{aligned}
\frac{d\phi_m}{dt} = s(1-\phi_n-\phi_m) - v\phi_m - b\phi_n^2\phi_m &= 0 \\
s - s\phi_n - s\phi_m - v\phi_m - b\phi_n^2 &= 0 \\
s\phi_n + b\phi_n^2\phi_m &= -v\phi_m - s\phi_m + s \\
(b\phi_m)\phi_n^2 + s\phi_n &= s - \phi_m(v+s) \\
(b\phi_m)\phi_n^2 + s\phi_n - [s - \phi_m(v+s)] &= 0\,.
\end{aligned}$$

The left-hand side is quadratic in ϕ_n, and thus we have

$$\phi_n = \frac{-s \pm \sqrt{s^2 + 4(b\phi_m)[s-\phi_m(v+s)]}}{2b\phi_m}\,. \tag{B.4}$$

Next we set B.3 equal to B.4 and solve for ϕ_m, as follows.

$$\begin{aligned}
\frac{d}{b\phi_m} &= \frac{-s \pm \sqrt{s^2 + 4(b\phi_m)[s - \phi_m(v+s)]}}{2b\phi_m} \\
2d &= -s \pm \sqrt{s^2 + 4(b\phi_m)[s - \phi_m(v+s)]} \\
2d + s &= \pm\sqrt{s^2 + 4(b\phi_m)[s - \phi_m(v+s)]} \\
(2d+s)^2 &= s^2 + 4(b\phi_m)[s - \phi_m(v+s)] \\
4d^2 + 4ds &= 4bs\phi_m - 4bv\phi_m^2 - 4bs\phi_m^2 \\
(4d^2 + 4ds) &= (4bs)\phi_m - \phi_m^2(4bv + 4bs) \\
0 &= (4bv + 4bs)\phi_m^2 - (4bs)\phi_m + (4d^2 + 4ds)
\end{aligned}$$

But this is quadratic in ϕ_m, so we have

$$\begin{aligned}
\phi_m &= \frac{4bs \pm \sqrt{16b^2s^2 - 4(4bv + 4bs)(4d^2 + 4ds)}}{2(4bv + 4bs)} \\
&= \frac{4bs \pm \sqrt{16b^2s^2 - 64(bv + bs)(d^2 + ds)}}{8(bv + bs)} \\
&= \frac{bs \pm \sqrt{b^2s^2 - 4(bv + bs)(d^2 + ds)}}{2(bv + bs)}\,.
\end{aligned}$$

Thus there are two equilibrium points at

$$\phi_m = \frac{bs + \sqrt{b^2s^2 - 4bd(v+s)(d+s)}}{2b(v+s)} \tag{B.5}$$

and

$$\phi_m = \frac{bs - \sqrt{b^2s^2 - 4bd(v+s)(d+s)}}{2b(v+s)}\,. \tag{B.6}$$

Examining the nullclines (see figure B.1 we see that B.6 identifies the stable equilibrium point $(\frac{bs-\sqrt{b^2s^2-4bd(v+s)(d+s)}}{2b(v+s)}, \frac{2d(v+s)}{bs-\sqrt{b^2s^2-4bd(v+s)(d+s)}})$, which is in agreement with the continuous (mean field) model.

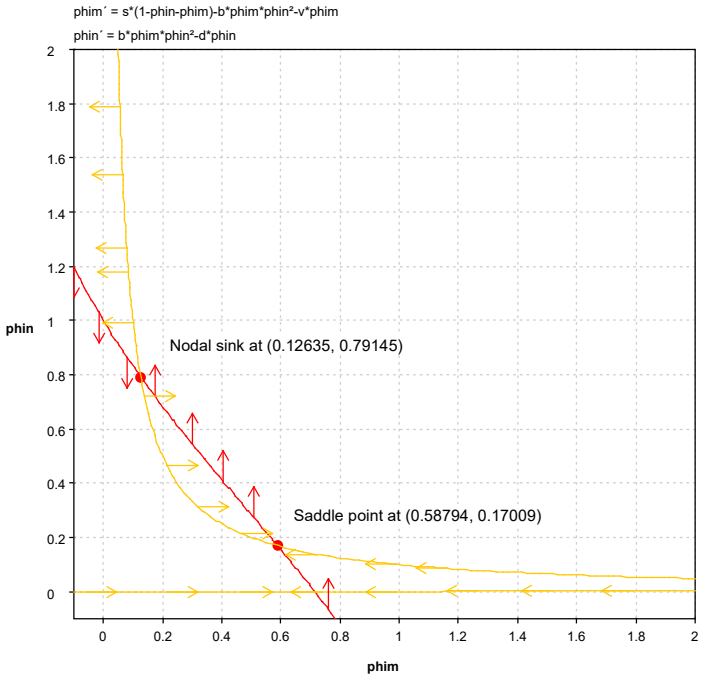

Fig. B.1: Nullclines and equilibrium points of stochastic model with parameter values $s = 2.5, d = 0.12, b = 1$ and $v = 1$.

For these parameter values, the Jacobian of the stable equilibrium is $\begin{bmatrix} -4.1264 & -2.7 \\ 0.6264 & 0.1 \end{bmatrix}$ and the eigenvalues and eigenvectors are:

$$\begin{aligned} -0.34756 \qquad & (0.58136, -0.81365) \\ -3.6788 \qquad & (-0.98654, 0.16353)\,. \end{aligned}$$

The Jacobian of the saddle point is $\begin{bmatrix} -3.5289 & -2.7 \\ 0.028929 & 0.1 \end{bmatrix}$ and the eigenvalues and eigenvectors are:

$$\begin{aligned} 0.078347 \qquad & (0.59922, -0.80058) \\ -3.5073, \qquad & (-0.99997, 0.0080195)\,. \end{aligned}$$

Appendix C

Future Work: The Stochastic Model with Space

In this appendix we derive an individual based model which includes space, thus vegetation diffusion and water advection are accounted for. We then use this to derive the mean-field and mesoscale equations, which may be used in future work.

C.1 Vegetation Diffusion

Consider now a planar lattice where each element is a patch within which the non-spatial dynamics described in the last Section holds. By selecting randomly two patches, say i and j, there are nine possibilities of further randomly choosing one individual from each. For describing vegetation movement we are only interested in the pairs $\{B, E\}$. Two migration events between the selected patches are then possible

$$B_iE_j \xrightarrow{\theta} E_iB_j, \quad E_iB_j \xrightarrow{\theta} B_iE_j, \tag{C.1}$$

with associated rate θ. We must also account for vegetation growth or death as before, with the following events and their associated rates and probabilities:

- $B_iW_i \xrightarrow{bn/N} W_iB_i = \frac{1}{\Omega}\frac{n_i^2}{N^2}\frac{m_i}{N-1}$
- $W_iB_i \xrightarrow{bn/N} B_iW_i = \frac{1}{\Omega}\frac{m_i}{N-1}\frac{n_i^2}{N^2}$
- $B_i \xrightarrow{d} E_i = \frac{1}{\Omega}\frac{n_i}{N}$,

where Ω is the number of patches in the lattice.

Let n_i and n_j denote the number of biomass units in the patches and z the number of neighbors of a patch. The transition probabilities for the vegetation migration events are

- $T(...n_i - 1...n_j + 1...|...n_i...n_j...) = \frac{\theta}{z\Omega}\frac{n_i}{N}\frac{N-m_j-n_j}{N}$
- $T(...n_i + 1...n_j - 1...|...n_i...n_j...) = \frac{\theta}{z\Omega}\frac{n_j}{N}\frac{N-m_i-n_i}{N}$

and the remaining transition probabilities are

- $T(...n_i+1, m_i...|...n_i, m_i...) = \frac{2b}{\Omega}\frac{n_i^2}{N^2}\frac{m_i}{N-1}$
- $T(...n_i-1, m_i...|...n_i, m_i...) = \frac{d}{\Omega}\frac{n_i}{N}$.

The associated Kolmogorov equation, which now includes spatial transitions, is then:

$$\begin{aligned}\frac{dP(\overrightarrow{n},\overrightarrow{m},t)}{dt} = \sum_i \sum_{j\in i} [&T(...n_i, n_j...|...n_i-1, n_j+1...)P(...n_i-1, n_j+1..., t)\\ &- T(...n_i+1, n_j-1...|...n_i, n_j...)P(...n_i, n_j..., t)\\ &+ T(...n_i, n_j...|...n_i+1, n_j-1...)P(...n_i+1, n_j-1..., t)\\ &- T(...n_i-1, n_j+1...|...n_i, n_j...)P(...n_i, n_j..., t)\\ &+ T(...n_i, m_i...|...n_i-1, m_i...)P(...n_i-1, m_i..., t)\\ &- T(...n_i+1, m_i...|...n_i, m_i...)P(...n_i, m_i..., t)\\ &+ T(...n_i, m_i...|...n_i+1, m_i...)P(...n_i+1, m_i..., t)\\ &- T(...n_i-1, m_i...|...n_i, m_i...)P(...n_i, m_i..., t)]\\ &\pm \textit{water transition probabilities}\,.\end{aligned}$$

Here the transition probabilities have been paired together for easier simplification. Note that as before, none of the transition probabilities including changes only in m are involved in the equation for $\frac{d\langle n\rangle}{dt}$.

We find the rate equation for vegetation by substituting the master equation into:

$$\frac{d\langle n_k\rangle}{dt} = \sum_{\overrightarrow{n}}\sum_{\overrightarrow{m}} n_k \frac{P(\overrightarrow{n},\overrightarrow{m},t)}{dt}$$

to obtain:

$$\begin{aligned}\frac{d\langle n_i\rangle}{dt} = \sum_{\overrightarrow{n}}\sum_{\overrightarrow{m}}\Bigg\{\Bigg[&\sum_i\sum_{j\in i}(n_i+1)T(...n_i+1, n_j-1...|...n_i, n_j...)\\ &- n_i T(...n_i+1, n_j-1...|...n_i, n_j...)\Bigg]P(...n_i, n_j..., t)\end{aligned}$$

$$
\begin{aligned}
&+\Bigg[\sum_i\sum_{j\in i}(n_i-1)T(...n_i-1,n_j+1...|...n_i,n_j...)\\
&\qquad\qquad -n_iT(...n_i-1,n_j+1...|...n_i,n_j...)\Bigg]P(...n_i,n_j...,t)\\
&+\Bigg[\sum_i(n_i+1)T(...n_i+1,m_i...|...n_i,m_i...)\\
&\qquad\qquad -n_iT(...n_i+1,m_i...|...n_i,m_i...)\Bigg]P(...n_i,m_i...,t)\\
&+\Bigg[\sum_i(n_i-1)T(...n_i-1,m_i...|...n_i,m_i...)\\
&\qquad\qquad -n_iT(...n_i-1,m_i...|...n_i,m_i...)\Bigg]P(...n_i,m_i...,t)\Bigg\},
\end{aligned}
$$

which reduces to:

$$
\begin{aligned}
\frac{d\langle n_i\rangle}{dt}=&\sum_{\overrightarrow{n}}\sum_{\overrightarrow{m}}\Bigg\{\Bigg[\sum_i\sum_{j\in i}T(...n_i+1,n_j-1...|...n_i,n_j...)\Bigg]P(...n_i,n_j...,t)\\
&-\Bigg[\sum_i\sum_{j\in i}T(...n_i-1,n_j+1...|...n_i,n_j...)\Bigg]P(...n_i,n_j...,t)\\
&+\Bigg[\sum_i T(...n_i+1,m_i...|...n_i,m_i...)\Bigg]P(...n_i,m_i...,t)\\
&+\Bigg[\sum_i -T(...n_i-1,m_i...|...n_i,m_i...)\Bigg]P(...n_i,m_i...,t)\Bigg\}.
\end{aligned}
$$

Recognizing expected values and substituting in the values for the transition rates yields

$$
\begin{aligned}
\frac{d\langle n_i\rangle}{dt}=&\sum_{j\in i}\frac{\theta}{z\Omega}\frac{\langle n_j\rangle}{N}\frac{(N-\langle n_i\rangle-\langle m_i\rangle)}{N}-\sum_{j\in i}\frac{\theta}{z\Omega}\frac{\langle n_i\rangle}{N}\frac{(N-\langle n_j\rangle-\langle m_j\rangle)}{N}\\
&+\frac{2b}{\Omega}\left(\frac{\langle n_i\rangle}{N}\right)^2\frac{\langle m_i\rangle}{N-1}-\frac{d}{\Omega}\frac{\langle n_i\rangle}{N}.
\end{aligned}
$$

Now let $\tilde{b}=\frac{2b}{N-1}$, $\tilde{d}=\frac{d}{N}$, rescale time to let $\tau=\frac{t}{\Omega}$ and then divide by N. Then,

$$
\frac{d\langle n_i\rangle}{d\tau}=\frac{\theta}{zN}\left[\sum_{j\in i}\frac{\langle n_j\rangle}{N}\frac{(N-\langle n_i\rangle-\langle m_i\rangle)}{N}-\frac{\langle n_i\rangle}{N}\frac{(N-\langle n_j\rangle-\langle m_j\rangle)}{N}\right]+...
$$

$$
\begin{aligned}
&\quad ... + \tilde{b}\left(\frac{\langle n_i\rangle}{N}\right)^2 \frac{\langle m_i\rangle}{N} - \tilde{d}\frac{\langle n_i\rangle}{N} \\
&= \frac{\theta}{zN}\left[\sum_{j\in i}\frac{\langle n_j\rangle}{N}\left(1-\frac{\langle n_i\rangle}{N}-\frac{\langle m_i\rangle}{N}\right) - \frac{n_i}{N}\left(1-\frac{\langle n_j\rangle}{N}-\frac{\langle m_j\rangle}{N}\right)\right] \\
&\quad + \tilde{b}\left(\frac{\langle n_i\rangle}{N}\right)^2 \frac{\langle m_i\rangle}{N} - \tilde{d}\frac{\langle n_i\rangle}{N} \\
&= \frac{\theta}{zN}\left[\sum_{j\in i}(\phi_j - \phi_i\phi_j - \phi_j\psi_i) - (\phi_i - \phi_i\phi_j - \phi_i\psi_j)\right] + \tilde{b}\phi_i^2\psi_i - \tilde{d}\phi_i\,,
\end{aligned}
$$

where $\phi_i = \frac{\langle n_i\rangle}{N}$, $\phi_j = \frac{\langle n_j\rangle}{N}$, $\psi_i = \frac{\langle m_i\rangle}{N}$ and $\psi_j = \frac{\langle m_j\rangle}{N}$.

This simplifies to

$$
\frac{d\langle n_i\rangle}{d\tau} = \frac{\theta}{zN}\left[\sum_{j\in i}(\phi_j - \phi_i - \phi_j\psi_i + \phi_i\psi_j)\right] + \tilde{b}\phi_i^2\psi_i - \tilde{d}\phi_i \tag{C.2}
$$

$$
= \frac{\theta}{N}\left[\frac{1}{z}\sum_{j\in i}(\phi_j - \phi_i) + \frac{1}{z}\sum_{j\in i}(\phi_i\psi_j - \phi_j\psi_i)\right] + \tilde{b}\phi_i^2\psi_i - \tilde{d}\phi_i \tag{C.3}
$$

$$
= \frac{\theta}{N}\left[\Delta\phi_i + \frac{1}{z}\sum_{j\in i}(\phi_i\psi_j - \phi_j\psi_i)\right] + \tilde{b}\phi_i^2\psi_i - \tilde{d}\phi_i\,, \tag{C.4}
$$

where Δ is the lattice Laplacian $\Delta\phi_i = \frac{1}{z}\sum_{j\in i}(f_j - f_i)$, and $\sum_{j\in i}$ represents the sum over the neighboring patches j. Noticing that $\phi_i\psi_j - \phi_j\psi_i = \phi_i(\psi_j - \psi_i) - \psi_i(\phi_j - \phi_i)$, the expression in brackets can be rewritten as

$$
\phi_i\Delta\psi_i - \psi_i\Delta\phi_i\,.
$$

The appearance of this cross-diffusion term is a consequence of the nature of the reactions (C.1), i.e. the requirement of space available where the individual is moving, [14]. If we assume that the capacity of each patch is much larger than the number of individuals, the cross-diffusion term is negligible and the mean-field equation for the biomass is approximated by

$$
\frac{d\langle n_i\rangle}{dt} = \frac{\theta}{\Omega N}\Delta\langle n_i\rangle + \tilde{b}\langle n_i\rangle^2\langle m_i\rangle - \tilde{d}\langle n_i\rangle\,. \tag{C.5}
$$

Letting lattice spacing tend to zero, i.e. carrying the problem into continuous space, gives

$$\partial_t \langle n \rangle = D\Delta \langle n \rangle + \tilde{b} \langle n \rangle^2 \langle m \rangle - \tilde{d} \langle n \rangle \ , \tag{C.6}$$

where $D = \theta/\Omega N$.

C.2 Water Advection

Another consequence of assuming a large capacity in each patch is that we can allow the unidirectional movement of water, which in our context has deterministic behavior and is produced by a small landscape gradient. Let us assume that the movement is made along the X axis. That the water moves with velocity ν means that at each time step $h = \epsilon/\nu$, where ϵ is the lattice spacing, a transition of the type

$$W_i E_j \to E_i W_j$$

is produced between the patches i and j, with the former being to the right of the latter and assuming that there is at least one element W in the i patch. Thus, the relation

$$\frac{\langle m_j \rangle - \langle m_i \rangle}{h} = \nu \frac{\langle m_j \rangle - \langle m_i \rangle}{\epsilon}$$

relating the relative changes due to advective movement leads to

$$\partial_t \langle m \rangle = \nu \partial_x \langle m \rangle$$

when ϵ tends to zero. Therefore, the mean field equation, i.e. total rate at which changes in water volume are produced, is given by combining the spatial and non-spatial effects (equation (8)),

$$\partial_t \langle m \rangle = \nu \partial_x \langle m \rangle + \tilde{s} - \tilde{b} \langle n \rangle^2 \langle m \rangle - \tilde{v} \langle m \rangle \ . \tag{C.7}$$

For large N, equations (11) and (12) constitute an approximation of Klausmeier's model from the stochastic model.

Recalling that $\langle n \rangle = N\phi_n$ and $\langle m \rangle = N\phi_m$, equations (11) and (12) can be written as

$$\partial_t \phi_n = D\Delta\phi_n + \tilde{b}N^2\phi_n^2\phi_m - \tilde{d}\phi_n, \tag{C.8}$$

$$\partial_t \phi_m = \nu\partial_x\phi_m + S - \tilde{b}N^2\phi_n^2\phi_m - \tilde{v}\phi_m\,, \tag{C.9}$$

where $S = \tilde{s}/N$ and $\tilde{b} = 2b/(N-1)$ again.

C.3 Mesoscale Equations

If i represents the spatial index then the mesoscale equations for the i^{th} patch in the lattice come from (13) and (14) as

$$\frac{d\phi_{ni}}{dt} = D\Delta^*\phi_{ni} + D\left(\phi_{ni}\Delta^*\phi_{mi} - \phi_{mi}\Delta^*\phi_{ni}\right) + \tilde{b}\phi_{ni}^2\phi_{mi} - \tilde{d}\phi_{ni}\,, \tag{C.10}$$

where $D = \theta/\Omega N$, $\tilde{b} = 2b/(N-1)$ and $\tilde{d} = d/N$, and

$$\frac{d\phi_{mi}}{dt} = \tilde{\nu}\left(\phi_{mj} - \phi_{mi}\right) + S(1 - (\phi_{ni} + \phi_{mi})) - \tilde{b}\phi_{ni}^2\phi_{mi} - \tilde{v}\phi_{mi}\,, \tag{C.11}$$

where $\tilde{\nu} = \nu N/\epsilon$, $S = \tilde{s}/N$, $\tilde{v} = v/N$ and the neighbor patch j is where water comes from.

Similarly to the non-spatial case, we obtain the expressions

$$\begin{aligned}
A_{ni}(\phi_i) &= D\Delta^*\phi_{ni} + D\left(\phi_{ni}\Delta^*\phi_{mi} - \phi_{mi}\Delta^*\phi_{ni}\right) + \tilde{b}\phi_{ni}^2\phi_{mi} - \tilde{d}\phi_{ni},\\
A_{mi}(\phi_i) &= \tilde{\nu}\left(\phi_{mj} - \phi_{mi}\right) + S(1 - (\phi_{ni} + \phi_{mi})) - \tilde{b}\phi_{ni}^2\phi_{mi} - \tilde{v}\phi_{mi},\\
B^i_{nn}(\phi_i) &= D\Delta^*\phi_{ni} + D\left(\phi_{ni}\Delta^*\phi_{mi} - \phi_{mi}\Delta^*\phi_{ni}\right) + \tilde{b}\phi_n^2\phi_m + \tilde{d}\phi_n,\\
B^i_{nm}(\phi_i) &= -\tilde{b}\phi_n^2\phi_m,\\
B^i_{mm}(\phi_i) &= \tilde{\nu}\left(\phi_{mj} - \phi_{mi}\right) + \tilde{b}\phi_n^2\phi_m + S(1 - \phi_n - \phi_m) + \tilde{v}\phi_m\,.
\end{aligned}$$

Appendix D

Additional Simulation Results

D.1 Simulation Results with $N = 10^4$.

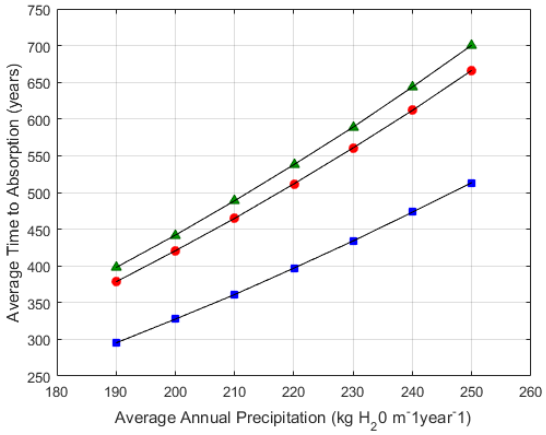

(a) Trees ($N = 10^4$)

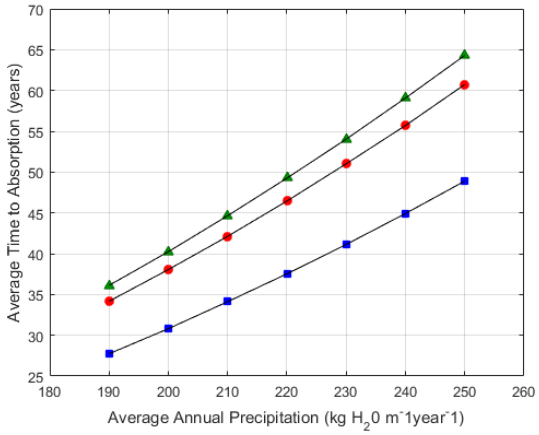

(b) Grass ($N = 10^4$)

Fig. D.1: Average time to extinction plotted against average annual precipitation with $N = 10^4$ and initial conditions $\phi(0) = (0.1, 0.1)$ (squares), $\phi(0) = (0.5, 0.5)$ (circles), and $\phi(0) = (0.9, 0.1)$ (triangles). Each time average was obtained from $50,000$ simulations.

Appendix E

MatLab Code

This appendix contains the codes used to create figures and tables in the thesis as explained in each of the following subsections.

E.1 Code for Figure 2.1

The following MatLab code creates Figure 2.1.

```
% Plots a stochastic simulation, a mean-field solution and
   klausmeier's
% model solution all on one graph.

clear all;

%% Stochastic Simulation
%============================% PARAMETERS AND VARIABLES
a=1;                          % precipitation (rescaled)
m=0.05;                       % veggie death rate (rescaled)
N=500;                        % patch capacity
T=1000;                       % time

p=1;                          % veggies
q=1;                          % water units
%============================%

t=0;
figure;
hold on;
i=1;

while (p>0 && q>=0 && t<=T);

    %============================% TRANSITION RATES
    TR1=p^2*q;                    %(p,q)-->(p+1,q-1)
    TR2=m*p;                      %(p,q)-->(p-1,q)
    TR3=a;                        %(p,q)-->(p,q+1)
    TR4=q;                        %(p,q)-->(p,q-1)

```

```
    TR=TR1+TR2+TR3+TR4;          % total rate of events

    Tpoints(i)=t;
    P(i)=p;

    t=t+exprnd(1/TR);

    r=rand;
    if r<TR1/TR;
        p=p+1; q=q-1;
    elseif and(TR1/TR<=r,r<(TR1+TR2)/TR);
        p=p-1;
    elseif and((TR1+TR2)/TR<=r,r<(TR1+TR2+TR3)/TR);
        q=q+1;
    else and((TR1+TR2+TR3)/TR<=r,r<1);
        q=q-1;
    end

    if q<0
        q=0;
    end

    if p==0;
        T=t;
        break;
    end

    i=i+1;

end

plot(Tpoints,P,'r')%,t,q,'b')

axis([0 T 0 40]);
root1=a/(2*m)+sqrt((a/(2*m))^2-1)
root2=a/(2*m)-sqrt((a/(2*m))^2-1)

%%  Klausmeier's solution without space in blue dots
%  ode45 (function name, vector of time span, initial
   conditions which is a vector for more than one variable)

[t,dx]=ode45(@klauss,[0 1000],[1 1]);

plot(t,dx(:,1),'b:')

xlabel('time (rescaled)')
```

```
75 ylabel('<n>')
76 hold on
77
78 %% Our Mean-field Model in black dash-dots
79
80 %  ode45 (function name, vector of time span, initial
      conditions which is a vector for more than one variable)
81
82 [t,dx]=ode45(@klaus,[0 1000],[1 1]);
83
84 plot(t,dx(:,1),'k-.')
```

E.2 Code(s) for Figures 3.2 and D.1

This first code runs 50,000 simulations of the mesoscale model, computing the extinction times and returning the mean. It simulates real data and creates the histogram found in Figure 3.2.

```
% TimetoDesert.m
% Euler-Maruyama method for solving stochastic differential equations
% SDE is dphin=An dt + (1/sqrtN)*(gnn*dW1)
% and dphim=Am dt + (1/sqrtN)*(gmn*dW1+gmm*dw2)
% where An=b*phin^2*phim-d*phin and
% Am=S(1-phin-phim)-b*phin^2*phim-v*phim
% gnn=some function,and gnm=some function,
% phin(0)=phin0=?VARIES

% Discretized Brownian path over [0,500] has dt=500/2^(11), which is approx 0.2441
% Euler-Maruyama uses timestep R*dt

clear all

K=500;                      % patch size--the number of individuals in the patch, or thecapacity of the patch
% Klausmeier Parameters for Grass
A = 250;                    % annual precipitation
RR = 100;                   % water uptake by plants
LL = A/75;                  % evaporation rate
J = 0.003;                  % yield of plant biomass
M = 1.8;                    % mortality rate

% Klausmeier Parameters for Trees
% A = 200;                  % annual precipitation
% RR = 1.5;                 % water uptake by plants
% LL = A/75;                % evaporation rate
% J = 0.002;                % yield of plant biomass
% M = 0.18;                 % mortality rate

AVT = [];                   % empty matrix to hold the time to extinction for each trial k.
T=500; N=2^11; dt=T/N;      % T is the final time; N is the number of intervals; dt is the change in time or length of the intervals
                            % Note here that we are working in terms of
```

```
33                          % Tau=t/K, or time divided by the
                               system size,
34                          % thus we need to scale by a factor
                               of K, and
35                          % choose N accordingly, to keep the
                               step size
36                          % small.  Our choice of N=2^11
                               yields
37                          % comparable calculations to this
                               scaling.
38 R=1; Dt=R*dt; L=N/R;     % L EM steps of size Dt=R*dt
39
40 B=J*sqrt(RR)/LL^(3/2); % part of parameter a (S)--controls
      water input
41 d=M/LL;       % parameter m--measures plant losses (d tilde)
42 b=1;                   % constants b tilde, v tilde and S(s)
43 v=1;
44 s=A*B;
45
46
47 for k=1:50000;
48
49 %randn('state',1);          % Sets the state for repeatable
      experiments
50 dW1=sqrt(dt)*randn(1,N);    % Brownian increments for dW1
51 W1=cumsum(dW1);             % discretized Brownian path
52
53 %randn('state',50);
54 dW2=sqrt(dt)*randn(1,N);    % Brownian increments for dW2
55 W2=cumsum(dW2);
56
57 phinEM=zeros(1,L);    % preallocating vectors of length L for
      phin/phim for E-M method
58 phimEM=zeros(1,L);
59
60 % INITIAL CONDITIONS
61 phin0=0.1;      % initial plant density <n>/K; must be <1.
62 phim0=0.1;      % initial water density
63
64 phinEM(1)=phin0;      %  The first entry of the vectors are
      the initial conditions
65 phimEM(1)=phim0;
66
67 phintemp=phin0;       % a temporary holding for the values
      generated
68 phimtemp=phim0;
```

```
69
70  for j=1:L
71
72      Winc1=sum(dW1(R*(j-1)+1:R*j));
73      Winc2=sum(dW2(R*(j-1)+1:R*j));
74
75      gnn=sqrt(b*phintemp^2*phimtemp+d*phintemp);
76      gnm=0;
77      gmn=-1*(b*phintemp^2*phimtemp)/(sqrt(b*phintemp^2*phimtemp
           +d*phintemp));
78      gmm=sqrt(b*phintemp^2*phimtemp+s*(1-phintemp-phimtemp)+v*
           phimtemp-(b*phintemp^2*phimtemp)^2/(b*phintemp^2*
           phimtemp+d*phintemp));
79
80      phintemp=phintemp+Dt*(b*phintemp^2*phimtemp-d*phintemp)
           +(1/sqrt(K))*(gnn*Winc1);
81
82      phimtemp=phimtemp+Dt*(s*(1-phintemp-phimtemp)-b*phintemp
           ^2*phimtemp-v*phimtemp)+(1/sqrt(K))*(gmn*Winc1+gmm*
           Winc2);
83
84      if phimtemp<0
85          phimtemp=0;
86      end
87
88      % If phintemp <=0, then the vegetation is gone, thus the
           time to extinction is on the next time step (j+1), call
           this ExT
89      if phintemp<=0
90          ExT = j+1;
91          phinEM(j+1)=0;
92          phin = phinEM(1:ExT);
93          phim = phimEM(1:ExT);
94          AVT(end+1) = ExT*Dt*LL; % This ExT becomes the Last
               entry in our time vector after we scale the time
               back to normal time by multiplying by LL (what we
               scaled time by originally)
95          break;
96      end
97
98      phinEM(j+1)=phintemp;
99      phimEM(j+1)=phimtemp;
100
101     ExT = L;
102 end
103
```

```
104 if ExT==L
105     ExT=L+1;
106     phin = phinEM;
107     phim = phimEM;
108 end
109 end
110
111 %dlmwrite('A190.txt',AVT');     % Copies the data from AVT
       into a data file
112 figure(1)
113 % Creates a histogram of the values in AVT, the times to
       extinction for each trial run k.
114 histogram(AVT,'Normalization','probability');
115
116 xlabel('Average Time to Absorption (in years) for Grass','
       FontSize',11)
117 ylabel('Probability','FontSize',11)
118 legend('210 kg H_20 m^-2year^-1','250 kg H_20 m^-2year^-1')
119 MEAN=mean(AVT)          % Returns the mean time to extinction
120 STD=std(AVT)            % Returns the standard deviation of the
        times to extinction
121 hold on
122
123 %figure(2);
124 % Creates a plot of the density of veg and water vs. time
125 %plot(LL*[0:Dt:(ExT-1)*Dt],phin,'r');
126 %hold on
127 %plot(LL*[0:Dt:(ExT-1)*Dt],phim,'b');
128 %xlabel('time (years)','FontSize',12);
129 %ylabel('<n>','FontSize',16,'Rotation',0,'HorizontalAlignment
       ','right');
130 %grid on
```

The following code uses the data created by the previous code to create Figures 3.2 and D.1.

```
% TimeToDesertGraphs.m
% Creates graphs which plot the average time to bare-soil against average
% annual precipitation.

clear all;

% For N=500...

% TREES
TS=[189.5016 209.9826 231.5614 254.6912 278.4560 303.6373 329.6891;
    272.0442 302.4873 335.0714 368.4437 404.5689 441.5589 481.0018;
    291.5214 323.5984 358.2973 395.7213 433.4615 473.5001 515.7965];

figure(1)                                % Trees Plot
plot([190:10:250],TS(1,:),'Color','b','Marker','s','MarkerFaceColor','b')
hold on
plot([190:10:250],TS(1,:),'k-');
hold on
plot([190:10:250],TS(2,:),'Color','r','Marker','o','MarkerFaceColor','r')
hold on
plot([190:10:250],TS(2,:),'k-');
hold on
plot([190:10:250],TS(3,:),'Color',[0 .4 0],'Marker','^','MarkerFaceColor',[0 .6 0]);
hold on
plot([190:10:250],TS(3,:),'k-')
axis([180 260 150 550]);
hold on
xlabel('Average Annual Precipitation (kg H_20 m^-1year^-1)','FontSize',11);
ylabel('Average Time to Absorption (years)','FontSize',11);
grid on
%title('Trees, N=500')

% GRASS  [(0.1,0.1); (0.5,0.5); (0.9,0.1)]
GS=[18.0396 19.9986 22.1234 24.3316 26.6672 29.1333 31.6143;
```

```
35      24.4041 27.1582 30.0628 33.1678 36.4355 39.8458 43.3761;
36      26.3933 29.3614 32.5986 35.9455 39.4672 43.1419 47.0066];
37
38  figure(2)       % Grass Plot
39  plot([190:10:250],GS(1,:),'Color','b','Marker','s','
        MarkerFaceColor','b')
40  hold on
41  plot([190:10:250],GS(1,:),'k-');
42  hold on
43  plot([190:10:250],GS(2,:),'Color','r','Marker','o','
        MarkerFaceColor','r')
44  hold on
45  plot([190:10:250],GS(2,:),'k-');
46  hold on
47  plot([190:10:250],GS(3,:),'Color',[0 .4 0],'Marker','^','
        MarkerFaceColor',[0 .6 0]);
48  hold on
49  plot([190:10:250],GS(3,:),'k-')
50  axis([180 260 15 50])
51  hold on
52  %plot(LL*[0:Dt:(ExT-1)*Dt],phim,'b');
53  xlabel('Average Annual Precipitation (kg H_20 m^-1year^-1)','
        FontSize',11);
54  ylabel('Average Time to Absorption (years)','FontSize',11);
55  grid on
56  %title('Grass, N=500')
57
58  %% For N=10000...
59
60  % TREES
61  TS=[295.1249 327.5406 360.9405 396.9971 434.0354 473.2195
        513.3676;
62      378.3396 420.6367 464.7322 511.7594 560.7676 611.8188
           666.3537;
63      397.8612 441.8719 488.7622 537.9516 589.0216 643.7465
           700.6334];
64
65  figure(3)       % Trees Plot
66  plot([190:10:250],TS(1,:),'Color','b','Marker','s','
        MarkerFaceColor','b')
67  hold on
68  plot([190:10:250],TS(1,:),'k-');
69  hold on
70  plot([190:10:250],TS(2,:),'Color','r','Marker','o','
        MarkerFaceColor','r')
71  hold on
```

```
plot([190:10:250],TS(2,:),'k-');
hold on
plot([190:10:250],TS(3,:),'Color',[0 .4 0],'Marker','^','
   MarkerFaceColor',[0 .6 0]);
hold on
plot([190:10:250],TS(3,:),'k-')
axis([180 260 250 750]);
hold on
xlabel('Average Annual Precipitation (kg H_20 m^-1year^-1)','
   FontSize',11);
ylabel('Average Time to Absorption (years)','FontSize',11);
grid on
%title('Trees, N=10^4')

% GRASS  [(0.1,0.1); (0.5,0.5); (0.9,0.1)]
GS=[27.7312 30.8093 34.1190 37.5303 41.1317 44.9257 48.8976;
    34.1675 38.0533 42.1251 46.4505 51.0166 55.7105 60.7363;
    36.1142 40.2441 44.6512 49.2560 54.0398 59.0741 64.3077];

figure(4)                                % Grass Plot
plot([190:10:250],GS(1,:),'Color','b','Marker','s','
   MarkerFaceColor','b')
hold on
plot([190:10:250],GS(1,:),'k-');
hold on
plot([190:10:250],GS(2,:),'Color','r','Marker','o','
   MarkerFaceColor','r')
hold on
plot([190:10:250],GS(2,:),'k-');
hold on
plot([190:10:250],GS(3,:),'Color',[0 .4 0],'Marker','^','
   MarkerFaceColor',[0 .6 0]);
hold on
plot([190:10:250],GS(3,:),'k-')
axis([180 260 25 70])
hold on
%plot(LL*[0:Dt:(ExT-1)*Dt],phim,'b');
xlabel('Average Annual Precipitation (kg H_20 m^-1year^-1)','
   FontSize',11);
ylabel('Average Time to Absorption (years)','FontSize',11);
grid on
%title('Grass, N=10^4')
```

E.3 Code for Figure 4.1

The following code creates the plots found in Figure 4.1.

```
% TimeToDesertAgainstSystemCapacityGraph.m
% Figure(1) creates a plot of time to absorption as a function of the system capacity.
% Figure(2) is a plot of the difference between the curves in Figure(1).
% Matrix A holds values for time to absorption for Trees (with Initial
% Conditions (0.1, 0.1) and precipitation of 250 kg H_20 m^-2 year^-1
% for the system capacities listed in Matrix D (which are all x10^4).  Matrix B
% holds values with precipitation of 200 kg H_20 m^-2year^-1.
% N=500.
A=[1.6276 329.2826 372.0593 415.5715 429.1128 470.2861 496.4436 513.7356 527.1162 538.8384 548.0776 556.0340 563.9478 570.8132];

B=[1.3021 209.9534 237.2587 264.6408 273.5786 300.6575 316.0146 327.4661 336.0344 343.2827 349.3036 354.9180 359.1834 363.0663];

C=A-B;

D=[0 .05 .1 .2 .25 .5 .75 1 1.25 1.5 1.75 2 2.25 2.5];

figure(1)
plot(D(1,2:end),A(1,2:end),'k--')
hold on
plot(D(1,2:end),B(1,2:end),'k-.');
xlabel('N                                                    x10^4','FontSize',11,'HorizontalAlignment','left');
ylabel('Years','FontSize',11);
grid on

figure(2)            % Plots the difference
plot(D(1,2:end),C(1,2:end),'k-')
xlabel('N                                                    x10^4','FontSize',11,'HorizontalAlignment','left');
ylabel('Years','FontSize',11);
grid on
```